Biophysical modeling identifies an optimal hybrid amoeboid-mesenchymal phenotype for maximal T cell migration speeds

Roberto Alonso-Matilla[1-3], Paolo P. Provenzano[1-6] and David J. Odde[1-4*]

Affiliations:
[1]Department of Biomedical Engineering, University of Minnesota, Minneapolis, MN, USA
[2] University of Minnesota Physical Sciences in Oncology Center, Minneapolis, MN, USA
[3] University of Minnesota Center for Multiparametric Imaging of Tumor Immune Microenvironments, Minneapolis, MN, USA
[4] Masonic Cancer Center, University of Minnesota, USA
[5] Department of Hematology, Oncology, and Transplantation, University of Minnesota, USA
[6] Stem Cell Institute, University of Minnesota, USA

Classification:
PHYSICAL SCIENCES, Biophysics and Computational Biology

Keywords: Cell migration, biophysical model, amoeboid, bleb, actomyosin contractility

[*] Correspondence: oddex002@umn.edu

ABSTRACT — Many cell types, including transformed cells and immune cells, such as T cells, can produce protrusive, blister-like plasma membrane patches initially devoid of F-actin, called blebs. Despite recent progress in understanding the amoeboid-mesenchymal migration phenotype balance, it remains largely unknown how bleb-producing cells mechanically move through complex environments and what factors set their migration speed and directionality. Here, we have developed a hybrid stochastic-mean field biophysical model of bleb-based cell motility to study the potential for adhesion-free bleb-based migration. We find that simulated cells can only inefficiently migrate in the absence of adhesion-based forces, i.e., cell swimming, by producing high-to-low cortical contractility oscillations, where a high cortical contractility phase characterized by multiple bleb nucleation events is followed by an intracellular pressure buildup recovery phase at low cortical tensions, resulting in net cell motion. Our model suggests that bleb-producing cells can employ a hybrid bleb- and adhesion-based migration mechanism for optimum cell motility and identifies conditions for optimality. We find that blebs nucleate in subcellular regions of high cortical tension, low membrane-cortex linker density and high intracellular osmotic pressure. Lower extracellular matrix stiffnesses favor bleb growth, hence bleb-based cell swimming, which stands in contrast to classical mesenchymal/motor-clutch migration, where cell motility generally increases with increasing matrix stiffness. The developed model is expected to help generate design criteria for engineered immune therapies and provides a physical perspective of the potential migratory mechanisms underlying rapid single-cell migration, particularly in the context of bleb-based/amoeboid migration.

Significance Statement

T-cell based cancer therapies present a promising approach to treating cancer. Solid tumors create a highly immunosuppressive and fibrotic microenvironment that obstructs the infiltration of cytotoxic T cells, thus promoting tumor growth and metastasis. Despite recent progress, there is still a gap in our understanding of the migration mechanisms used by T cells to mechanically move through tissue. Here we determine that while cell shape deformation-based cell swimming is possibly used as a short-term exploratory mechanism, its predicted associated *in vivo* migration capabilities are suboptimal. Instead, our findings propose an alternative adhesion-based hybrid migration mechanism for optimal cell motility. This work provides important insights to aid design of cell engineering strategies to enhance migratory capabilities of antitumor immune cells.

Cell migration is a complex multistep process that is involved in major processes in the human body, acting as a driver of many morphogenetic events (1), as a regulator of tissue health and homeostasis (2), and associated with many diseases such as cancer, manifesting in cancer cell dissemination during metastasis (3) as well as in restricted immune cell migration within tumors (4). Cells migrating in three-dimensional environments use two dominant modes of migration: amoeboid and mesenchymal. The amoeboid phenotype is characterized by a rounded cellular morphology, high cortical contractility, low cell-matrix adhesions and narrow/tight extracellular spaces, and it is commonly associated with the formation of blebs (5-12), which are pressure driven spherical cellular membrane protrusions that are initiated by either a local membrane-cortex detachment or a local cortex rupture (13-15). This amoeboid blebby phenotype has been reported under some conditions for transformed cells from melanoma, breast cancer and squamous carcinoma cells *in vivo* (16-19), and is frequently displayed by T cells (20-22). The mesenchymal-like phenotype, which is frequently displayed by cancer cells from carcinomas under conducive conditions as well as fibrosarcoma and glioblastoma (23, 24), is characterized by an elongated morphology, strong cell-matrix adhesion, available space in the extracellular environment and the formation of actin-rich leading-edge structures such as spike-like filopodia or broad flattened lamellipodia (9, 11, 23, 25). In their lifetime, cells navigate through extremely complex microenvironments, such as tight porous viscoelastic tissues or narrow vascular pores. As a result, many cancer cells (11, 16, 26-31) and immune cells such as T cells (20) can extend both types of cellular protrusions, and adapt to different mechanical and chemical microenvironments by transitioning between mesenchymal and amoeboid migration modes.

T cell-based cancer therapies offer a promising approach in the fight against cancer. However, successful T cell-based clinical trials have been limited mainly to hematologic cancers. Solid tumors create a highly immunosuppressive and fibrotic microenvironment that hinders the physical infiltration and activity of cytotoxic T cells, facilitating tumor growth and metastasis (32, 33). Despite the significant progress in understanding bleb formation in recent years (20, 34, 35),

it remains largely unknown how bleb-producing T cells exchange momentum with their surroundings to navigate through challenging mechanical and chemical microenvironments such as tumors. Hence, a combination of biophysical modeling and cutting-edge experimental approaches is needed to elucidate T cell migration mechanisms and devise immune engineering strategies to enhance T cell infiltration, migration and sampling within the tumor mass, with the aim of advancing the next generation of treatments for solid tumors.

Adhesion-dependent migration has long been thought to be required for cell motility, but some recent findings have challenged this view (10, 25, 36-49). An alternative mechanism is bleb-based cell swimming. Most animal cells have a dense and thin actomyosin layer that lies underneath the plasma membrane and that produces cortical tension mediated forces that get transmitted to the membrane by membrane-cortex linker proteins, such as Ezrin, Radixin and Moesin proteins (50, 51). Upon a local membrane-cortex adhesion loss, cortical forces no longer get transmitted to the plasma membrane and a bleb nucleates and undergoes fast expansion reaching bleb sizes of 0.5-2 m. At the bleb nucleation site, the local hydrostatic pressure presumably drops, and cytoplasmic material flows from the center of the cell to the low-pressure bleb site (52, 53). The bleb cycle ends by the self-assembly of new cortex underneath the bleb membrane, which drives bleb retraction (13, 54). Yet, it is not obvious whether this form of cell motility requires cell-matrix adhesion interactions, nonspecific cell-matrix friction interactions or if the cell can achieve a net displacement after each bleb cycle in complete adhesion-independent conditions.

The theoretical study of bleb nucleation (55-61) and bleb growth (53, 62-64) has been studied using coarse-grained mechanistic models. A few amoeboid/bleb-based motility biophysical models have also been recently developed, where the intracellular and extracellular spaces were assumed to behave as viscous fluids (47, 48, 65-75). Most of these models assume that plasma membrane and cortex are a single composite material. Two of these studies, however account for the mechanical interactions between the intracellular viscous fluid, the actin cortex

and the cell membrane (65, 66). The model by Lim et al. (65) does not satisfy conservation of momentum, since it does not account for the forces exerted by the cortex on the cytoplasm as it moves through the crowded intracellular medium. The model of Copos and Strychalski (66) introduces a cortical viscoelastic force that depends on a reference cortical configuration, as well as a steric interaction force with the walls; and the inclusion of these two forces does not guarantee that the total force exerted by the cell on the medium vanishes, potentially violating conservation of linear momentum as well. In the present study, we develop a biophysical mechanistic model of bleb-based cell swimming in a viscoelastic medium to assess whether bleb-producing cells such as T cells can mechanically swim in the absence of adhesions, identify the key cellular components that regulate the motile capabilities of swimming cells and quantify the theoretical maximum speed that a cell can achieve using this migration mechanism. We determine that bleb-based cell swimming is theoretically possible but practically limited so that it is not a plausible *in vivo* mechanism. Rather, our results suggest an alternative hybrid model where blebbing mediates rapid protrusion extension and subsequent adhesion effectively captures the newly gained cell position. The biophysical model provides key insights to mechanically control and potentially maximize migration of blebby cells such as T cells that will hopefully contribute to the design of tumor stroma and cell-specific engineering strategies to enhance the migratory capabilities of antitumor immune cells.

RESULTS

Biophysical model of bleb-based cell swimming

We aim to investigate the cell migration capabilities of bleb-producing cells in an unbounded viscoelastic medium through the development of a two-dimensional biophysical mechanistic model (see Supplemental Material for a detailed description of the model). The cell is composed of two distinct structures: a cellular membrane and an actomyosin cortex (Fig. 1A). Both are

considered Lagrangian structures defined by a set of nodes that are connected to each other and the associated fluids as described below and in more detail in the supplement. As the cell migrates through the environment, both membrane and cortex structures transmit forces on the surrounding medium, generating viscoelastic stresses. At the continuum level, conservation of mass and momentum on the incompressible viscoelastic fluid reads

$$\nabla \cdot \mathbf{v}_{\mathrm{f}}(\mathbf{x}, \mathrm{t}) = 0 \qquad (1)$$

$$\nabla \cdot \boldsymbol{\sigma}_{\mathrm{tot}}(\mathbf{x}, \mathrm{t}) + \boldsymbol{\mathcal{F}}_{\mathrm{tot}}(\mathbf{x}, \mathrm{t}) = \mathbf{0} \qquad (2)$$

$$\boldsymbol{\mathcal{F}}_{\mathrm{tot}}(\mathbf{x}, \mathrm{t}) = \boldsymbol{\mathcal{F}}_{\mathbf{m}}(\mathbf{x}, \mathrm{t}) + \boldsymbol{\mathcal{F}}_{\mathbf{c,drag}}(\mathbf{x}, \mathrm{t}) \qquad (3)$$

where $\mathbf{v}_{\mathrm{f}}$ is the fluid velocity, $\boldsymbol{\sigma}_{\mathbf{tot}}$ is the total stress, $\boldsymbol{\mathcal{F}}_{\mathbf{tot}}$ is the total force density on the fluid and equal to the sum of the membrane force density $\boldsymbol{\mathcal{F}}_{\mathbf{m}}$ and cortical force density $\boldsymbol{\mathcal{F}}_{\mathbf{c,drag}}$ generated in the intracellular medium. The total stress $\boldsymbol{\sigma}_{\mathbf{tot}} = \boldsymbol{\sigma}_{\mathbf{f}} + \boldsymbol{\sigma}_{\mathbf{p}}$ is the sum of two contributions: a purely viscous stress $\boldsymbol{\sigma}_{\mathbf{f}}$ and a viscoelastic stress $\boldsymbol{\sigma}_{\mathbf{p}}$:

$$\boldsymbol{\sigma}_{\mathbf{f}} = -\boldsymbol{\nabla}\mathrm{p} + \eta_{\mathrm{f}}\left(\boldsymbol{\nabla}\mathbf{v}_{\mathbf{f}} + \boldsymbol{\nabla}\mathbf{v}_{\mathbf{f}}{}^{\mathbf{T}}\right) \qquad (4)$$

$$\boldsymbol{\sigma}_{\mathbf{p}} = \frac{\eta_{\mathrm{p}}(\mathbf{x}, \mathrm{t})}{\lambda_{\mathrm{p}}(\mathbf{x}, \mathrm{t})}\left[\left(\frac{\boldsymbol{\kappa}_{\mathbf{p}}}{1 - \mathrm{tr}\left(\boldsymbol{\kappa}_{\mathbf{p}}\right)/\mathrm{L}_{\mathrm{p}}^{2}}\right) - \mathbf{I}\right] \qquad (5)$$

where we have chosen the FENE-P constitutive relation for the stress to model the viscoelastic nature of the intracellular and extracellular spaces (76). Here, p is the hydrostatic pressure, η_{f} and η_{p} are, respectively, the fluid viscosity and polymer viscosity, λ_{p} is the polymer stress relaxation time, $\boldsymbol{\kappa}_{\mathbf{p}}$ is the conformation stress tensor and L_{p} is the polymer extensibility parameter, a measure of the maximum polymeric deformation. The time evolution of the conformation stress tensor $\boldsymbol{\kappa}_{\mathbf{p}}$ reads

$$\frac{\partial \boldsymbol{\kappa}_{\mathbf{p}}}{\partial \mathrm{t}} = \frac{1}{\lambda_{\mathrm{p}}}\left(\mathbf{I} - \frac{\boldsymbol{\kappa}_{\mathbf{p}}}{1 - \mathrm{tr}\left(\boldsymbol{\kappa}_{\mathbf{p}}\right)/\mathrm{L}_{\mathrm{p}}^{2}}\right) - \mathbf{v}_{\mathbf{f}} \cdot \boldsymbol{\nabla}\boldsymbol{\kappa}_{\mathbf{p}} + \boldsymbol{\nabla}\mathbf{v}_{\mathbf{f}}{}^{\mathbf{T}} \cdot \boldsymbol{\kappa}_{\mathbf{p}} + \boldsymbol{\kappa}_{\mathbf{p}} \cdot \boldsymbol{\nabla}\mathbf{v}_{\mathbf{f}} \qquad (6)$$

The first term on the right-hand side (RHS) of Eq. (6) captures stress relaxation kinetics, the second term captures polymer advection, and the last two terms capture rotation and deformation of the polymeric material.

The cell membrane is an elastic structure subjected to tension, bending and membrane-cortex adhesion forces, and the cortex is considered an actomyosin poroelastic structure that generates myosin-mediated forces that obey a linear force-velocity relationship and create tension in the cortical network (58, 77-79). The actin cortex experiences drag forces as cytoplasmic material flows through the porous actomyosin network. Mass conservation of membrane-cortex linkers, and actin and myosin in the cortex follows simple stochastic association and dissociation kinetics. No-slip between the plasma membrane and viscoelastic fluids is enforced. Furthermore, the model accounts for osmotic effects. The intracellular osmotic pressure resists cortex and extracellular osmotic inward forces, all forces combined set cell size and shape. A hypothetical complete depletion of intracellular osmolyte would cause a sudden cell shrinkage within a few milliseconds (Fig. 1B).

Single bleb formation, expansion and retraction does not allow cells to swim

We proceed to study cell dynamics during a single bleb cycle by enforcing local membrane-cortex detachment. Membrane-cortex uncoupling is followed by a drop in local intracellular hydrostatic pressure and cytoplasmic viscoelastic fluid material flows through the detached actomyosin meshwork from the center of the cell to the low-pressure region, mediating bleb expansion (Figs. 2A, B, and movie 1). The poroelastic permeable cortex does not sustain pressure forces and moves retrogradely towards the cell center (80, 81), with cortical inward forces balanced by cytoplasm-mediated drag forces. Eventually, cortex components disappear via turnover kinetics (i.e. first-order disassembly without concomitant assembly; see Eqs. S20-21). The bleb cycle ends by recruitment of new cortex constituents underneath the bleb membrane, which nucleates new actin filaments, that recruit myosin motors that transmit inward forces to the plasma membrane

driving bleb retraction and cytoplasm from the bleb region to the center of the cell in a low intracellular hydrostatic pressure gradient phase (Figs. 2A, B). Cell shape-based swimming of microscale biological cells (i.e. at low Reynolds number) requires non-reciprocal body deformations to generate locomotion (82). We observe that the plasma membrane follows similar trajectories during bleb expansion and bleb retraction. A forward movement of cytoplasmic material translocates the center of mass of the cell forward in the direction of the bleb during bleb growth, and a rearward movement of cytoplasmic material translocates the center of mass of the cell in the opposite direction during bleb retraction, thus net cell displacements at the end of a single bleb cycle are negligible (Figs. 2C−E). Overall, our results indicate that expansion and retraction of individual blebs is nearly a time-reversible process and does not cause net cell displacements.

High intracellular hydrostatic pressure gradients and low elastic stresses favor bleb expansion

Next, we employed the model to define how different cellular conditions influence cell displacements during bleb growth. The cell produces viscoelastic stresses on its surroundings as blebs expand/retract. The spatial structure of these stresses is examined in Figs. (2C, inset) and (S2A), where high polymer stresses concentrate at the front of the cell providing an additional resistance to pressure-driven bleb expansion, resulting in lower cell displacements for extracellular materials with a low stress relaxation time λ_p^{out}. Therefore, softer (high λ_p^{out}) and less dense (low polymer viscosity η_p^{out}) cellular environments favor bleb growth (Figs. 2C and S2B). This is consistent with the frequent formation of blebs in open extracellular spaces and soft environments (20, 83), suggesting that bleb-producing cells may use this mechanism to navigate structurally and mechanically heterogenous microenvironments. In a similar way, softer and less

dense intracellular fluids favor larger cell displacements during bleb expansion (Fig. S2C), indicating that intracellular crowdedness penalizes cell translocation during bleb growth by resisting cytoplasmic material flows. Interestingly, bleb expansion rates obtained from Fig. (2C) ($\sim 5.3\ \mu\mathrm{m/s}$ and $\sim 10.8\ \mu\mathrm{m/s}$ for $\lambda_{\mathrm{p}}^{\mathrm{out}} = 0.1\mathrm{s}$, and $\lambda_{\mathrm{p}}^{\mathrm{out}} = 100\mathrm{s}$, respectively) are at least an order of magnitude higher than diffusion-limited polymerization rates of monomeric G-actin into F-actin $\sim 200\ \mathrm{nm/s}$ (84-86), which drive filopodial and lamellipodial extension, suggesting that maximal cell migration speeds might involve bleb expansion dynamics. For a given bleb size, more contractile and softer actomyosin cortices favor larger cell displacements during bleb expansion (Figs. 2D and 2E), respectively. High cortical squeezing, mediated by a higher number of myosin motors in the cell, causes larger intracellular hydrostatic pressure gradients after membrane-cortex dissociation, driving stronger cytoplasmic flows and larger bleb sizes and cell displacements during cell forward motion. A softer cortex gives rise to stronger intracellular flows (Fig. S1A) and delays intracellular hydrostatic pressure equilibration and the end of bleb expansion (Fig. S1B) due to its intrinsic slow viscoelastic relaxation time. Maximal cell displacements during bleb expansion are also achieved for intermediate membrane-cortex detachment sizes (Fig. S2D) as they cause stronger and highly polarized back-to-front cytoplasmic flows. Other cellular conditions that cause maximal cell displacements during bleb growth include high cortex porosity as a highly porous cortex has less mechanical resistance to pressure-driven cytoplasmic flows through the cortical meshwork (Fig. S2E), and low plasma membrane tension as membrane tension builds up at the cell front during bleb growth thus opposing further expansion (Fig. S2A) and a softer membrane provides less elastic resistance to forward plasma membrane motion, as shown in Fig. S2F. Overall, our model results show that larger cell displacements during bleb growth are favored by soft and low-density extracellular and intracellular spaces, soft and highly porous actomyosin cortices, high myosin motor levels, intermediate bleb sizes and softer plasma membranes.

Sustained adhesion-free bleb-based cell swimming requires cortical contractility oscillations

We next explored whether bleb-producing cells can swim in adhesion-free conditions by producing bleb-based cell shape changes. To embrace more complex variations in the dynamics of cortex component amounts we introduce stochasticity in the kinetics of membrane-cortex linkers, actin and myosin, where membrane-cortex linkers stochastically associate in a force-independent manner and unbind by force with an effective dissociation rate that increases exponentially with force according to Bell's law (87) (see Supplemental Material for additional details). Hereinafter, we consider intracellular and extracellular spaces to be viscous fluids to estimate maximum bleb-based cell migration capabilities. We find that bleb-producing cells that maintain a consistent high contractility level cannot effectively migrate, as shown by the plateau reached by the sample average mean-squared displacement-time curve after a few bleb nucleation events (Fig. 3A and movie 2). The significant cell displacement achieved by the cells during the first bleb cycles suggests that cells could potentially migrate starting from a healed cortex with a fully pressurized intracellular cytoplasm. Therefore, we introduced a cortical contractility oscillator signal into the model, to mimic cortical contractility oscillations (88, 89), and allow the cortex to recover and "heal" before initiating the next bleb cycle. We find that cells are capable of swimming by producing high-to-low cortical contractility oscillations, where a high cortical tension phase characterized by multiple bleb nucleation events is followed by an intracellular pressure buildup recovery phase at low cortical contractility, resulting in mean-squared cell displacements that increase over time (Fig. 3B). Intermediate frequencies of the cortical oscillation signal seem to maximize cell swimming migratory capabilities (Fig. 3C). Overall, these results show that adhesion-free bleb-based cell shape changes combined with high-to-low cortical tensions are a possible strategy by which cells could migrate through biological tissues or fluids via a stochastic swimming behavior of repeated cycles of bleb-based protrusions driven by oscillations in cortical contractility.

Maximal bleb-based migratory potential achieved for high myosin motors and a soft cortex

We next explore the optimum cellular conditions for maximal cell spreading via the oscillatory bleb-based swimming mechanism identified above. We identify two important model parameters that strongly modulate cell migration capabilities: cortical stiffness and cortical tension. We find that a soft cortex is essential for cell motility (Figs. 4A and 4B). Cortical stiffnesses per unit of actin κ_c higher than $\sim 0.2\ \mathrm{pN}/\mu\mathrm{m}$ give rise to extremely low random cell motility coefficients, as shown in Fig. (4B). For an estimated number of actin units at each cortical node of $\bar{n}_{act} \sim 2 \times 10^4$ (see Supplemental Information), our model result predicts that a cell with a cortical stiffness greater than 4000 $\mathrm{pN}/\mu\mathrm{m}$ cannot swim effectively. Quantitative analysis shows a biphasic behavior of bleb nucleation frequency ν_{bleb} as a function of cortical stiffness, with a minimum nucleation frequency found at intermediate cortical stiffnesses, as depicted in Figs. (4C) and (4D). Intermediate bleb nucleation frequencies correlate with maximal cell random motility coefficients (Fig. (4D)). Whereas cells cannot swim under low-frequency conditions, since effectively cells nucleate a sequence of isolated bleb cycles, leading to no swimming, as already discussed and shown in Fig. (2), high-frequency blebby cells are not capable of successfully pressurizing their cytoplasm between consecutive bleb events, causing a decrease in their swimming propulsion efficiency. Intermediate blebbing frequencies are therefore ideal conditions for swimming, where the synchronized nucleation of multiple blebs indeed allows cells to break time-reversibility and effectively migrate in the absence of adhesion-based forces. Interestingly, metastatic potential of prostate cancer cells correlate with reduced F-actin and high blebbing frequency (90). The polar angle between consecutive bleb nucleation events, here referred to as bleb nucleation correlation angle p_{bleb}, monotonically decreases with cortex stiffness, as shown in Fig. (4E), with soft-cortex cells and stiff-cortex cells nucleating blebs at $p_{bleb} \sim [60^o - 70^o]$ and $p_{bleb} < 40^o$, respectively, as depicted in Fig. (4F).

We additionally find that high cortical contractility is essential for bleb-based cell motility, with high-myosin-motor cells possessing a higher migration potential than low-myosin-motor cells, as depicted by the mean-squared displacement curves, effective random motility coefficients and wind rose migratory cell track (Figs. (4G, H and S3), respectively. Higher number of myosin motors increases blebbing frequency and bleb nucleation correlation angle (Figs. 4I–L). Maximal cell motility coefficients not only correlate with intermediate blebbing frequencies (as already discussed) but also with intermediate bleb-to-bleb polar angles, as shown in the scatter plots in Figs. (4J) and (4L). Maximal cell motility coefficients correlate with bleb nucleation frequencies of $\nu_{\mathrm{bleb}} \sim 4s^{-1}$ and bleb-to-bleb polar angles of $\mathrm{p}_{\mathrm{bleb}} \sim 60^{\mathrm{o}}$. Cells that nucleate sequential blebs with low correlation angles ($\mathrm{p}_{\mathrm{bleb}} < 40^{\mathrm{o}}$), i.e. blebs on top of blebs, approach geometrical reciprocal motion resulting in vanishing cell motility coefficients, whereas cells that nucleate sequential blebs too separated from each other spatially ($\mathrm{p}_{\mathrm{bleb}} > 70^{\mathrm{o}}$) lose directionality/cell polarization, do not create effective non-reciprocal plasma membrane deformations and their migratory potential is penalized, as Fig. (4L) shows. Whereas slow turnover time of cortex components, low fluid viscosity and low membrane tension favor bleb-based cell spreading, we have not observed any statistically significant difference in migration capabilities for the different values explored of cortex porosity, as depicted in Fig. (S4). We hypothesize that the actomyosin cortical meshwork hinders cytoplasmic flows during both bleb expansion and bleb retraction, and so the slowdown of cytoplasmic flows during both phases cancels out and its effect on bleb-based cell spreading becomes insignificant. Overall, our model results show that cells with a soft cortex and elevated cortical tension exhibit more efficient migration by extending large bleb protrusions and the precise spatiotemporal nucleation of blebs, suggesting that engineering therapeutic T cells to possess increased cortical tension and/or a softer cortex would favor bleb-based T cell movement in complex environments. Notably, our cortical tension result is consistent with recent experimental findings, where high contractility pushed adhesive T cells into a faster amoeboid phenotype (20).

Blebs nucleate in regions of high cortical tension, low membrane-cortex linker density and high intracellular osmotic pressure

We investigate the role of spatial variations in mechanical factors that potentially control the location of bleb nucleation sites, and thus bleb-based cell directionality. Bleb initiation is initiated by either a local decrease in membrane-cortex adhesion or by a local cortex tear. Either way, failure of membrane-cortex linkers or F-actin associated linker proteins must precede and initiate bleb nucleation events. We explore three different cellular conditions: spatially dependent cortical myosin recruitment, spatially dependent membrane-cortex linker recruitment, and asymmetric distribution of ion pumps within the plasma membrane. Blebs preferentially form in regions of high cortical contractility (high myosin) and low membrane-cortex linker levels, as shown in Fig. (5A), and in agreement with experimental observations (21, 91, 92). Linkers preferentially reach a high tensional state in areas of myosin enrichment, as they are subjected to higher cortical inward forces that eventually cause them to dissociate by force in a runaway process, giving rise to local membrane-cortex detachment and bleb formation. In a similar way, linkers located in low linker density regions are overpowered by high cortical loads making them more susceptible to failure. The highly polarized orientational distribution of blebbing events forces cells to extend protrusions along one axis, restricting their motion to only one degree of freedom, and in turn impeding their migration as shown in Fig. (5B) and consistent with the scallop theorem (82). Therefore, enforcing the formation of blebs in a small cell region turns out to be a poor cell shape change-based swimming strategy. Linker failure is also exacerbated in high intracellular osmotic pressure regions (Fig. (S5)). The highly porous cortex does not sustain net osmotic forces, therefore an increase in local intracellular osmotic pressure causes membrane outward motion, straining linkers which eventuates in a cascade of linker failures and bleb formation. Overall, our model results show that a competition between membrane-cortex adhesion and a combination of osmotic and cortical forces control the location of bleb formation sites.

Rapid cell migration is potentially enabled by a hybrid bleb- and adhesion-based mode of migration for optimum cell motility

In this section, we explore whether blebbing alone can mediate efficient cell migration in the absence of adhesion-based forces, namely bleb-based cell swimming, or if it requires adhesion interactions with the environment for optimal motility. We find that bleb-based coordinated cell-scale deformations are inefficient and lead to maximal migration motility coefficients of $\sim 1.5\ \mu m^2/min$ (Fig. 4), an order of magnitude lower than reported *in vivo* cell motility coefficients of bleb-producing cells such as T cells (44), which display much faster speeds than those achieved by mesenchymal cells (93). In such poor swimming conditions, interstitial flows may be dominant in certain tissues over the inherent swimming motion of cells rendering cell swimming less relevant to cell translocation (94, 95).

Next, we investigate the effect of cell-environment adhesion interactions on the migration capabilities of bleb-producing adherent cells by constructing a simple hybrid adhesion-based, bleb-based cell migration biophysical model (Fig. 6A, see Supplemental Material for a detailed description of the model). Our findings indicate that adhesion interactions with the environment significantly increase cell migration speeds, with cells being capable of translocating approximately up to $d_{exp} \sim 0.4\ \mu m$ during an isolated bleb cycle (Figs. 6B, C). In this mode of migration, we observe that blebbing allows cells to push their cell front forward at a very fast rate ($\sim 10\ \mu m/s$), much faster than F-actin polymerization rates and consistent with experimental observations (80), followed by formation of focal adhesions at the cell front, which prevents cell rearward motion during bleb retraction and mediates subsequent traction force generation and fast forward cell translocation. Our model shows that bleb producing adherent cells migrate more effectively under high cortical tension conditions (Fig. 6B). Interestingly, while a softer cortex

favors greater cell displacements during bleb expansion, a stiffer cortex causes larger cell displacements during bleb retraction, with the highest net cell displacements occurring at intermediate cortical stiffnesses (Fig. 6C). Repeated cycles of adhesion-based blebbing dynamics can lead to diffusive cell behavior. Assuming that bleb nucleation sites are independent of the location of previous bleb nucleation events, we can estimate the 3D effective cell dispersion coefficient as $\mathrm{D_{cell}} = \mathrm{v_{cell}^2 t_{run}}/4$ (96), where cells run at an effective velocity given by $\mathrm{v_{cell}} = \mathrm{d_{exp}}/\mathrm{t_{run}}$ during an effective runtime $\mathrm{t_{run}}$. Given that reported blebbing frequencies are on the order of $\sim 4\mathrm{s}^{-1}$(80), we assume that the time needed for the cell to translocate during each bleb cycle is the limiting factor in each cell run; thus $\mathrm{t_{run}} \sim 0.3\mathrm{s}$ (Figs. 6A, B). Under these assumptions, $\mathrm{D_{cell}} = \mathrm{d_{exp}^2}/(4\mathrm{t_{run}}) = 60 \times (0.4\ \mu\mathrm{m})^2/(4 \times 0.3\mathrm{min}) = 8\mu\mathrm{m}^2/\mathrm{min}$. This value is comparable to the *in-vivo* motility coefficient of bleb-producing cells, suggesting that the hybrid cell migration mechanism might be a viable mode of migration for T cells navigating through tissues. Notice that enhanced traction forces mediated by actin polymerization forces have not been considered in this analysis and they will potentially enhance significantly the cell migratory potential of adherent blebby cells. However, how cells coordinate assembly and disassembly of focal adhesions, actin polymerization and traction forces with blebbing remains unclear.

In summary, our findings uncover potential mechanisms that are unlikely (i.e. swimming model) or possible (i.e. hybrid model) to mediate the remarkable ability of T cells to rapidly navigate through tissues. Our analysis does not support an adhesion-free swimming strategy based on changes in their cell shape, specifically through the formation of protruding blebs. This mechanism allows them to slowly explore the surrounding microenvironments. Instead, our analysis suggests that fast migration requires the presence of cell-environment adhesion interactions. Synergy between fast forward plasma membrane motion driven by bleb expansion and cell-matrix adhesion formation and subsequent traction force production potentially maximizes the migration potential of T cells. Adherent blebby cells can enhance their hybrid

migration capabilities by increasing cortical contractility and optimizing their cortical stiffness to an intermediate value.

DISCUSSION

We have introduced a mechanistic model of adhesion-free bleb-based cell migration to elucidate the physical principles and potential molecular components that modulate bleb-based cell swimming capabilities and identify how these molecular regulators can be perturbed to modulate their swimming potential. The amoeboid cellular phenotype has been associated with immune cell migration (20, 21, 97) as well as with multiple cancer cells displaying epithelial to amoeboid transitions with enhanced cell invasion, immunosuppression, stem cell potential and metastatic capabilities (98-102). Although the developed model is aimed at providing insights to effectively engineer therapeutic T cells with enhanced migration capabilities, the model's applicability extends broadly to all bleb-producing cells, including amoeboid cancer cells, with a major goal being to induce fast amoeboid T cell migration and target/inhibit amoeboid cancer cell migration.

Our model results indicate that sustained adhesion-free bleb-based cell motility requires oscillatory cortical forces, where cells alternate between a high-contractility motility phase and a low-contractility pressure buildup phase. These pulsatile actomyosin forces, which can arise from different mechanochemical sources, including calcium signal fluctuations (89, 103), myosin phosphorylation-based biochemical oscillators (104, 105), and ERK-based mechanochemical signaling, among others, do not seem to be essential in bleb-based cell swimming only, but also in other biological contexts including adhesion-based cell migration (88), compaction (106), cell intercalations (89) and tissue integrity (105) during morphogenesis, and temporal regulation of actin polymerization and vesicle exocytosis (103). Our analysis gives a new physical perspective of the mechanism underlying potential swimming of bleb-producing cells and provides a strategy to modulate cell swimming potential by targeting cortical contractility oscillations.

Repeated sequences of a single bleb nucleation event, bleb expansion, cortex recruitment and bleb retraction do not cause sustained cell swimming since the plasma membrane follows similar paths during bleb expansion and retraction. However, we show that spatiotemporal synchronization of multiple bleb nucleation events allows cells to break time-reversibility and effectively migrate in the absence of adhesion-based forces. Although cell signaling might play an important role in the coordination of multiple blebbing events, cells can orchestrate blebbing and control bleb frequency and bleb-to-bleb distance by temporal modulation of cortical tension and stiffness, where high tension and soft cortex favor optimum conditions. This is consistent with experiments, where high cortical contractility is associated with fast amoeboid-like cell motility (23, 30, 107). Motor activity levels can be modulated by the internal cellular state as well as by environmental cellular conditions. As an example, nuclear deformation mediated by enhanced cellular confinement can activate mechanotransduction pathways (108, 109) that enhance actomyosin contractility and therefore would be predicted to increase cell swimming potential. Whereas low contractile cells nucleate blebs at low frequencies and in regions near recent bleb nucleation sites, high contractile cells nucleate blebs at $\sim 4\mathrm{Hz}$ and cause membrane-cortex detachment at bleb-to-bleb separation polar angles of $\sim 60^{\mathrm{o}}$. These blebbing frequencies and bleb-to-bleb separation distances correlate with maximal cell motility coefficients.

In addition, our model shows that blebbing events are expected to be favored in cell regions of high cortical forces, low membrane-cortex adhesion and local intracellular osmotic swelling. This is consistent with experimental data, where blebbing was less frequent in the ezrin/radixin/moesin-rich uropod-like structure of cells (27, 110-112) and favored in calcium-dependent high myosin contraction regions at the leading edge of cells (12). Chemoattractants, which have also been associated with bleb polarization (113-115), potentially modulate some of the three driving factors mentioned above. Interestingly, we find that unidirectional bleb-based cell swimming is not possible via highly polarized bleb nucleation events, strongly suggesting that

persistent unidirectional cell migration, observed in different confined systems (10, 25, 41, 116) might require the presence of cellular frictional/adhesive forces with the environment (37, 42).

Maximal spreading of bleb-producing swimming cells is achieved for low-viscosity environments and low membrane tension. Our model results strongly suggest that low-density and softer extracellular environments favor bleb-based swimming. Additionally, our results indicate that coordinated cell-scale deformations driven by blebs are inefficient and result in maximal migration motility coefficients an order of magnitude lower than those reported by bleb-producing cells *in vivo*. Other possible adhesion-free cell swimming mechanisms rely on peristaltic waves (117), osmotic pressure (118), Marangoni stresses (47, 48) or slippage between plasma membrane and surrounding fluid (119) possibly caused by mechanical coupling of transmembrane proteins, powered by actin retrograde flows, with the surrounding fluid (38, 46).

We show that cells might employ a hybrid migration mechanism that combines blebbing and the formation of cell-matrix adhesions for optimal cell motility. Our results indicate that we can push adherent blebby T cells into a highly migratory phenotype by increasing their contractility and fine-tuning their cortical stiffness to intermediate values. This mode of migration is consistent with a recent study that shows that T cells push and pull on the extracellular matrix and require adhesion-based forces to migrate through *in vitro* systems (120). It is also consistent with another cell migration study, where recruitment of the branched actin nucleator Arp2/3 frequently follows membrane-cortex detachment, depletion of the ERM membrane-cortex linker ezrin and protrusion expansion (92). In some instances, however, cell-extracellular matrix adhesion formation and blebbing events anticorrelate in space, potentially suggesting the presence of adhesion-only-driven protrusions or pressure-only-driven protrusions (121). Recent modeling results also suggest that cortical squeezing at the cell rear combined with focal adhesion formation at the cell front is a fast and robust cell migration strategy (122). It is unclear though how blebbing, actin polymerization forces, traction forces, and spatial dynamics of focal adhesion assembly and disassembly integrate all together.

Overall, our work provides a new physical perspective of the possible mechanisms underlying the migration of blebby cells such as T cells and some cancer cells. The developed model provides not only strategies to enhance exploratory bleb-based T cell swimming but also suggested that pushing cells into a hybrid bleb- and adhesion-based mode of migration is a promising engineering strategy to increase T cell migration in tumors. A more rigorous study is needed to investigate to what extent this hybrid mode of migration can be adopted by T cells *in vivo*, which presents an exciting avenue for prospective theoretical and experimental research. To achieve this, advanced imaging, cell engineering and quantitative analysis combined with biophysical modeling will be indispensable in uncovering cell-specific and context-specific migration mechanisms. Ultimately, a faithful model could be used to define optimal states for maximal T cell migration and maximally effective immune cell therapies, and thereby guide the development of genetically engineered T cells optimized to migrate through mechanically challenging tumor microenvironments.

1. P. Friedl, D. Gilmour, Collective cell migration in morphogenesis, regeneration and cancer. *Nat Rev Mol Cell Biol* **10**, 445-457 (2009).
2. N. K. Karamanos, A. D. Theocharis, T. Neill, R. V. Iozzo, Matrix modeling and remodeling: A biological interplay regulating tissue homeostasis and diseases. *Matrix Biol* **75-76**, 1-11 (2019).
3. H. Yamaguchi, J. Wyckoff, J. Condeelis, Cell migration in tumors. *Curr Opin Cell Biol* **17**, 559-564 (2005).
4. A. Nicolas-Boluda, E. Donnadieu, Obstacles to T cell migration in the tumor microenvironment. *Comp Immunol Microbiol Infect Dis* **63**, 22-30 (2019).
5. M. Goudarzi *et al.*, Identification and regulation of a molecular module for bleb-based cell motility. *Dev Cell* **23**, 210-218 (2012).
6. V. Sanz-Moreno, C. J. Marshall, The plasticity of cytoskeletal dynamics underlying neoplastic cell migration. *Curr Opin Cell Biol* **22**, 690-696 (2010).
7. M. Ibo, V. Srivastava, D. N. Robinson, Z. R. Gagnon, Cell Blebbing in Confined Microfluidic Environments. *PLoS One* **11**, e0163866 (2016).
8. J. S. Logue *et al.*, Erk regulation of actin capping and bundling by Eps8 promotes cortex tension and leader bleb-based migration. *Elife* **4**, e08314 (2015).
9. S. Patel *et al.*, Myosin II and Arp2/3 cross-talk governs intracellular hydraulic pressure and lamellipodia formation. *Mol Biol Cell* **32**, 579-589 (2021).
10. V. Ruprecht *et al.*, Cortical contractility triggers a stochastic switch to fast amoeboid cell motility. *Cell* **160**, 673-685 (2015).

11. M. Bergert, S. D. Chandradoss, R. A. Desai, E. Paluch, Cell mechanics control rapid transitions between blebs and lamellipodia during migration. *Proc Natl Acad Sci U S A* **109**, 14434-14439 (2012).
12. H. Blaser *et al.*, Migration of zebrafish primordial germ cells: a role for myosin contraction and cytoplasmic flow. *Dev Cell* **11**, 613-627 (2006).
13. G. T. Charras, C. K. Hu, M. Coughlin, T. J. Mitchison, Reassembly of contractile actin cortex in cell blebs. *J Cell Biol* **175**, 477-490 (2006).
14. E. K. Paluch, E. Raz, The role and regulation of blebs in cell migration. *Curr Opin Cell Biol* **25**, 582-590 (2013).
15. G. Charras, E. Paluch, Blebs lead the way: how to migrate without lamellipodia. *Nat Rev Mol Cell Biol* **9**, 730-736 (2008).
16. M. Tozluoğlu *et al.*, Matrix geometry determines optimal cancer cell migration strategy and modulates response to interventions. *Nat Cell Biol* **15**, 751-762 (2013).
17. E. Sahai, C. J. Marshall, Differing modes of tumour cell invasion have distinct requirements for Rho/ROCK signalling and extracellular proteolysis. *Nat Cell Biol* **5**, 711-719 (2003).
18. K. Wolf *et al.*, Compensation mechanism in tumor cell migration: mesenchymal-amoeboid transition after blocking of pericellular proteolysis. *J Cell Biol* **160**, 267-277 (2003).
19. D. Rösel *et al.*, Up-regulation of Rho/ROCK signaling in sarcoma cells drives invasion and increased generation of protrusive forces. *Mol Cancer Res* **6**, 1410-1420 (2008).
20. E. D. Tabdanov *et al.*, Engineering T cells to enhance 3D migration through structurally and mechanically complex tumor microenvironments. *Nat Commun* **12**, 2815 (2021).
21. A. Takesono, S. J. Heasman, B. Wojciak-Stothard, R. Garg, A. J. Ridley, Microtubules regulate migratory polarity through Rho/ROCK signaling in T cells. *PLoS One* **5**, e8774 (2010).
22. P. Obeidy *et al.*, Partial loss of actin nucleator actin-related protein 2/3 activity triggers blebbing in primary T lymphocytes. *Immunol Cell Biol* **98**, 93-113 (2020).
23. P. Friedl, Prespecification and plasticity: shifting mechanisms of cell migration. *Curr Opin Cell Biol* **16**, 14-23 (2004).
24. B. L. Bangasser *et al.*, Shifting the optimal stiffness for cell migration. *Nat Commun* **8**, 15313 (2017).
25. Y. J. Liu *et al.*, Confinement and low adhesion induce fast amoeboid migration of slow mesenchymal cells. *Cell* **160**, 659-672 (2015).
26. V. Sanz-Moreno *et al.*, Rac activation and inactivation control plasticity of tumor cell movement. *Cell* **135**, 510-523 (2008).
27. A. Lorentzen, J. Bamber, A. Sadok, I. Elson-Schwab, C. J. Marshall, An ezrin-rich, rigid uropod-like structure directs movement of amoeboid blebbing cells. *J Cell Sci* **124**, 1256-1267 (2011).
28. P. Friedl, K. Wolf, Tumour-cell invasion and migration: diversity and escape mechanisms. *Nat Rev Cancer* **3**, 362-374 (2003).
29. M. L. Taddei, E. Giannoni, G. Comito, P. Chiarugi, Microenvironment and tumor cell plasticity: an easy way out. *Cancer Lett* **341**, 80-96 (2013).
30. K. Panková, D. Rösel, M. Novotný, J. Brábek, The molecular mechanisms of transition between mesenchymal and amoeboid invasiveness in tumor cells. *Cell Mol Life Sci* **67**, 63-71 (2010).

31. K. Saito, Y. Ozawa, K. Hibino, Y. Ohta, FilGAP, a Rho/Rho-associated protein kinase-regulated GTPase-activating protein for Rac, controls tumor cell migration. *Mol Biol Cell* **23**, 4739-4750 (2012).
32. E. Lanitis, D. Dangaj, M. Irving, G. Coukos, Mechanisms regulating T-cell infiltration and activity in solid tumors. *Ann Oncol* **28**, xii18-xii32 (2017).
33. C. Y. Slaney, M. H. Kershaw, P. K. Darcy, Trafficking of T cells into tumors. *Cancer Res* **74**, 7168-7174 (2014).
34. M. F. Krummel, F. Bartumeus, A. Gérard, T cell migration, search strategies and mechanisms. *Nat Rev Immunol* **16**, 193-201 (2016).
35. P. Nordenfelt, H. L. Elliott, T. A. Springer, Coordinated integrin activation by actin-dependent force during T-cell migration. *Nat Commun* **7**, 13119 (2016).
36. T. Lämmermann *et al.*, Rapid leukocyte migration by integrin-independent flowing and squeezing. *Nature* **453**, 51-55 (2008).
37. M. Bergert *et al.*, Force transmission during adhesion-independent migration. *Nat Cell Biol* **17**, 524-529 (2015).
38. P. R. O'Neill *et al.*, Membrane Flow Drives an Adhesion-Independent Amoeboid Cell Migration Mode. *Dev Cell* **46**, 9-22.e24 (2018).
39. S. E. Malawista, A. de Boisfleury Chevance, Random locomotion and chemotaxis of human blood polymorphonuclear leukocytes (PMN) in the presence of EDTA: PMN in close quarters require neither leukocyte integrins nor external divalent cations. *Proc Natl Acad Sci U S A* **94**, 11577-11582 (1997).
40. J. Renkawitz *et al.*, Adaptive force transmission in amoeboid cell migration. *Nat Cell Biol* **11**, 1438-1443 (2009).
41. A. K. Yip, K. H. Chiam, P. Matsudaira, Traction stress analysis and modeling reveal that amoeboid migration in confined spaces is accompanied by expansive forces and requires the structural integrity of the membrane-cortex interactions. *Integr Biol (Camb)* **7**, 1196-1211 (2015).
42. A. Reversat *et al.*, Cellular locomotion using environmental topography. *Nature* **582**, 582-585 (2020).
43. E. Woolf *et al.*, Lymph node chemokines promote sustained T lymphocyte motility without triggering stable integrin adhesiveness in the absence of shear forces. *Nat Immunol* **8**, 1076-1085 (2007).
44. M. Hons *et al.*, Chemokines and integrins independently tune actin flow and substrate friction during intranodal migration of T cells. *Nat Immunol* **19**, 606-616 (2018).
45. N. P. Barry, M. S. Bretscher, Dictyostelium amoebae and neutrophils can swim. *Proc Natl Acad Sci U S A* **107**, 11376-11380 (2010).
46. L. Aoun *et al.*, Amoeboid Swimming Is Propelled by Molecular Paddling in Lymphocytes. *Biophys J* **119**, 1157-1177 (2020).
47. H. Wu, M. A. P. de León, H. G. Othmer, Getting in shape and swimming: the role of cortical forces and membrane heterogeneity in eukaryotic cells. *J Math Biol* **77**, 595-626 (2018).
48. Q. Wang, H. G. Othmer, Computational analysis of amoeboid swimming at low Reynolds number. *J Math Biol* **72**, 1893-1926 (2016).
49. E. K. Paluch, I. M. Aspalter, M. Sixt, Focal Adhesion-Independent Cell Migration. *Annu Rev Cell Dev Biol* **32**, 469-490 (2016).

50. R. G. Fehon, A. I. McClatchey, A. Bretscher, Organizing the cell cortex: the role of ERM proteins. *Nat Rev Mol Cell Biol* **11**, 276-287 (2010).
51. R. Nambiar, R. E. McConnell, M. J. Tyska, Control of cell membrane tension by myosin-I. *Proc Natl Acad Sci U S A* **106**, 11972-11977 (2009).
52. M. Goudarzi, A. Boquet-Pujadas, J. C. Olivo-Marin, E. Raz, Fluid dynamics during bleb formation in migrating cells in vivo. *PLoS One* **14**, e0212699 (2019).
53. W. Strychalski, R. D. Guy, Intracellular Pressure Dynamics in Blebbing Cells. *Biophys J* **110**, 1168-1179 (2016).
54. N. Taneja, D. T. Burnette, Myosin IIA drives membrane bleb retraction. *Mol Biol Cell* **30**, 1051-1059 (2019).
55. C. Fang, T. H. Hui, X. Wei, X. Shao, Y. Lin, A combined experimental and theoretical investigation on cellular blebbing. *Sci Rep* **7**, 16666 (2017).
56. R. Alert, J. Casademunt, Bleb Nucleation through Membrane Peeling. *Phys Rev Lett* **116**, 068101 (2016).
57. A. Boulbitch *et al.*, Shape instability of a biomembrane driven by a local softening of the underlying actin cortex. *Phys Rev E Stat Phys Plasmas Fluids Relat Interdiscip Topics* **62**, 3974-3985 (2000).
58. J. Y. Tinevez *et al.*, Role of cortical tension in bleb growth. *Proc Natl Acad Sci U S A* **106**, 18581-18586 (2009).
59. F. Y. Lim, K. H. Chiam, L. Mahadevan, The size, shape, and dynamics of cellular blebs. *Europhysics Letters* **100** (2012).
60. L. L. Norman *et al.*, Cell blebbing and membrane area homeostasis in spreading and retracting cells. *Biophys J* **99**, 1726-1733 (2010).
61. J. Brugués *et al.*, Dynamical organization of the cytoskeletal cortex probed by micropipette aspiration. *Proc Natl Acad Sci U S A* **107**, 15415-15420 (2010).
62. T. E. Woolley *et al.*, Cellular blebs: pressure-driven, axisymmetric, membrane protrusions. *Biomech Model Mechanobiol* **13**, 463-476 (2014).
63. W. Strychalski, R. D. Guy, A computational model of bleb formation. *Math Med Biol* **30**, 115-130 (2013).
64. J. Young, S. Mitran, A numerical model of cellular blebbing: a volume-conserving, fluid-structure interaction model of the entire cell. *J Biomech* **43**, 210-220 (2010).
65. F. Y. Lim, Y. L. Koon, K. H. Chiam, A computational model of amoeboid cell migration. *Comput Methods Biomech Biomed Engin* **16**, 1085-1095 (2013).
66. C. Copos, W. Strychalski, Actin Turnover Required for Adhesion-Independent Bleb Migration. *Fluids* **7** (2022).
67. D. C. Bottino, L. J. Fauci, A computational model of ameboid deformation and locomotion. *Eur Biophys J* **27**, 532-539 (1998).
68. E. J. Campbell, P. Bagchi, A computational model of amoeboid cell motility in the presence of obstacles. *Soft Matter* **14**, 5741-5763 (2018).
69. E. J. Campbell, P. Bagchi, A computational study of amoeboid motility in 3D: the role of extracellular matrix geometry, cell deformability, and cell-matrix adhesion. *Biomech Model Mechanobiol* **20**, 167-191 (2021).
70. S. Dalal, A. Farutin, C. Misbah, Amoeboid swimming in a compliant channel. *Soft Matter* **16**, 1599-1613 (2020).
71. A. Farutin *et al.*, Amoeboid swimming: a generic self-propulsion of cells in fluids by means of membrane deformations. *Phys Rev Lett* **111**, 228102 (2013).

72. A. Moure, H. Gomez, Computational model for amoeboid motion: Coupling membrane and cytosol dynamics. *Phys Rev E* **94**, 042423 (2016).
73. H. Wu *et al.*, Amoeboid motion in confined geometry. *Phys Rev E Stat Nonlin Soft Matter Phys* **92**, 050701 (2015).
74. H. Wu *et al.*, Amoeboid swimming in a channel. *Soft Matter* **12**, 7470-7484 (2016).
75. J. P. Binagia, C. J. Guido, E. S. G. Shaqfeh, Three-dimensional simulations of undulatory and amoeboid swimmers in viscoelastic fluids. *Soft Matter* **15**, 4836-4855 (2019).
76. K. D. Housiadas, A. N. Beris, Polymer-induced drag reduction: Effects of the variations in elasticity and inertia in turbulent viscoelastic channel flow. *Physics of Fluids* **15**, 2369-2384 (2003).
77. P. Chugh *et al.*, Actin cortex architecture regulates cell surface tension. *Nat Cell Biol* **19**, 689-697 (2017).
78. P. Chugh, E. K. Paluch, The actin cortex at a glance. *J Cell Sci* **131** (2018).
79. T. M. Svitkina, Actin Cell Cortex: Structure and Molecular Organization. *Trends Cell Biol* **30**, 556-565 (2020).
80. B. Maugis *et al.*, Dynamic instability of the intracellular pressure drives bleb-based motility. *J Cell Sci* **123**, 3884-3892 (2010).
81. A. Grebecki, Dynamics of the contractile system in the pseudopodial tips of normally locomoting amoebae, demonstrated in vivo by video-enhancement. *Protoplasma* **154**, 98-111 (1990).
82. E. M. Purcell, Life at low Reynolds number. *American Journal of Physics* **45**, 3-11 (1977).
83. K. Wolf, R. Müller, S. Borgmann, E. B. Bröcker, P. Friedl, Amoeboid shape change and contact guidance: T-lymphocyte crawling through fibrillar collagen is independent of matrix remodeling by MMPs and other proteases. *Blood* **102**, 3262-3269 (2003).
84. T. D. Pollard, Rate constants for the reactions of ATP- and ADP-actin with the ends of actin filaments. *J Cell Biol* **103**, 2747-2754 (1986).
85. M. Yu *et al.*, mDia1 senses both force and torque during F-actin filament polymerization. *Nat Commun* **8**, 1650 (2017).
86. J. R. Kuhn, T. D. Pollard, Real-time measurements of actin filament polymerization by total internal reflection fluorescence microscopy. *Biophys J* **88**, 1387-1402 (2005).
87. G. I. Bell, Models for the specific adhesion of cells to cells. *Science* **200**, 618-627 (1978).
88. S. H. Lee *et al.*, A molecular clock controls periodically driven cell migration in confined spaces. *Cell Syst* **13**, 514-529.e510 (2022).
89. H. Tao *et al.*, Oscillatory cortical forces promote three dimensional cell intercalations that shape the murine mandibular arch. *Nat Commun* **10**, 1703 (2019).
90. Z. S. Khan, J. M. Santos, N. G. Vaz, F. Hussain, Enhanced blebbing as a marker for metastatic prostate cancer. *Biomicrofluidics* **13**, 034110 (2019).
91. E. Asante-Asamani *et al.*, A role for myosin II clusters and membrane energy in cortex rupture for Dictyostelium discoideum. *PLoS One* **17**, e0265380 (2022).
92. E. S. Welf *et al.*, Actin-Membrane Release Initiates Cell Protrusions. *Dev Cell* **55**, 723-736.e728 (2020).
93. P. Friedl, S. Borgmann, E. B. Bröcker, Amoeboid leukocyte crawling through extracellular matrix: lessons from the Dictyostelium paradigm of cell movement. *J Leukoc Biol* **70**, 491-509 (2001).

94. K. M. Kingsmore *et al.*, MRI analysis to map interstitial flow in the brain tumor microenvironment. *APL Bioeng* **2** (2018).
95. C. T. Curley *et al.*, Augmentation of brain tumor interstitial flow via focused ultrasound promotes brain-penetrating nanoparticle dispersion and transfection. *Sci Adv* **6**, eaay1344 (2020).
96. H. C. Berg, *Random walks in biology* (Princeton University Press, 1993).
97. P. Friedl, B. Weigelin, Interstitial leukocyte migration and immune function. *Nat Immunol* **9**, 960-969 (2008).
98. V. Graziani, I. Rodriguez-Hernandez, O. Maiques, V. Sanz-Moreno, The amoeboid state as part of the epithelial-to-mesenchymal transition programme. *Trends Cell Biol* 10.1016/j.tcb.2021.10.004 (2021).
99. A. Emad *et al.*, Superior breast cancer metastasis risk stratification using an epithelial-mesenchymal-amoeboid transition gene signature. *Breast Cancer Res* **22**, 74 (2020).
100. E. Crosas-Molist *et al.*, The NADPH oxidase NOX4 represses epithelial to amoeboid transition and efficient tumour dissemination. *Oncogene* **36**, 3002-3014 (2017).
101. Y. Gao *et al.*, Loss of ERα induces amoeboid-like migration of breast cancer cells by downregulating vinculin. *Nat Commun* **8**, 14483 (2017).
102. E. Giannoni *et al.*, EphA2-mediated mesenchymal-amoeboid transition induced by endothelial progenitor cells enhances metastatic spread due to cancer-associated fibroblasts. *J Mol Med (Berl)* **91**, 103-115 (2013).
103. N. Takeshita *et al.*, Pulses of Ca2+ coordinate actin assembly and exocytosis for stepwise cell extension. *Proc Natl Acad Sci U S A* **114**, 5701-5706 (2017).
104. X. Qin *et al.*, A biochemical network controlling basal myosin oscillation. *Nat Commun* **9**, 1210 (2018).
105. C. G. Vasquez, M. Tworoger, A. C. Martin, Dynamic myosin phosphorylation regulates contractile pulses and tissue integrity during epithelial morphogenesis. *J Cell Biol* **206**, 435-450 (2014).
106. J. L. Maître, R. Niwayama, H. Turlier, F. Nédélec, T. Hiiragi, Pulsatile cell-autonomous contractility drives compaction in the mouse embryo. *Nat Cell Biol* **17**, 849-855 (2015).
107. T. Lämmermann, M. Sixt, Mechanical modes of 'amoeboid' cell migration. *Curr Opin Cell Biol* **21**, 636-644 (2009).
108. A. J. Lomakin *et al.*, The nucleus acts as a ruler tailoring cell responses to spatial constraints. *Science* **370** (2020).
109. V. Venturini *et al.*, The nucleus measures shape changes for cellular proprioception to control dynamic cell behavior. *Science* **370** (2020).
110. S. Martinelli *et al.*, Ezrin/Radixin/Moesin proteins and flotillins cooperate to promote uropod formation in T cells. *Front Immunol* **4**, 84 (2013).
111. J. Rossy, M. C. Gutjahr, N. Blaser, D. Schlicht, V. Niggli, Ezrin/moesin in motile Walker 256 carcinosarcoma cells: signal-dependent relocalization and role in migration. *Exp Cell Res* **313**, 1106-1120 (2007).
112. V. Niggli, J. Rossy, Ezrin/radixin/moesin: versatile controllers of signaling molecules and of the cortical cytoskeleton. *Int J Biochem Cell Biol* **40**, 344-349 (2008).
113. P. D. Langridge, R. R. Kay, Blebbing of Dictyostelium cells in response to chemoattractant. *Exp Cell Res* **312**, 2009-2017 (2006).
114. M. Doitsidou *et al.*, Guidance of primordial germ cell migration by the chemokine SDF-1. *Cell* **111**, 647-659 (2002).

115. E. Zatulovskiy, R. R. Kay, Chemotactic Blebbing in Dictyostelium Cells. *Methods Mol Biol* **1407**, 97-105 (2016).
116. P. Maiuri *et al.*, Actin flows mediate a universal coupling between cell speed and cell persistence. *Cell* **161**, 374-386 (2015).
117. A. Franz, W. Wood, P. Martin, Fat Body Cells Are Motile and Actively Migrate to Wounds to Drive Repair and Prevent Infection. *Dev Cell* **44**, 460-470.e463 (2018).
118. K. M. Stroka *et al.*, Water permeation drives tumor cell migration in confined microenvironments. *Cell* **157**, 611-623 (2014).
119. H. A. Stone, A. D. Samuel, Propulsion of Microorganisms by Surface Distortions. *Phys Rev Lett* **77**, 4102-4104 (1996).
120. A. Caillier, D. Oleksyn, D. J. Fowell, J. Miller, P. W. Oakes (2023) T cells Use Focal Adhesions to Pull Themselves Through Confined Environments. (bioRxiv: the preprint server for biology), p 562587.
121. Y. Beckham *et al.*, Arp2/3 inhibition induces amoeboid-like protrusions in MCF10A epithelial cells by reduced cytoskeletal-membrane coupling and focal adhesion assembly. *PLoS One* **9**, e100943 (2014).
122. O. Maxian, A. Mogilner, W. Strychalski, Computational estimates of mechanical constraints on cell migration through the extracellular matrix. *PLoS Comput Biol* **16**, e1008160 (2020).

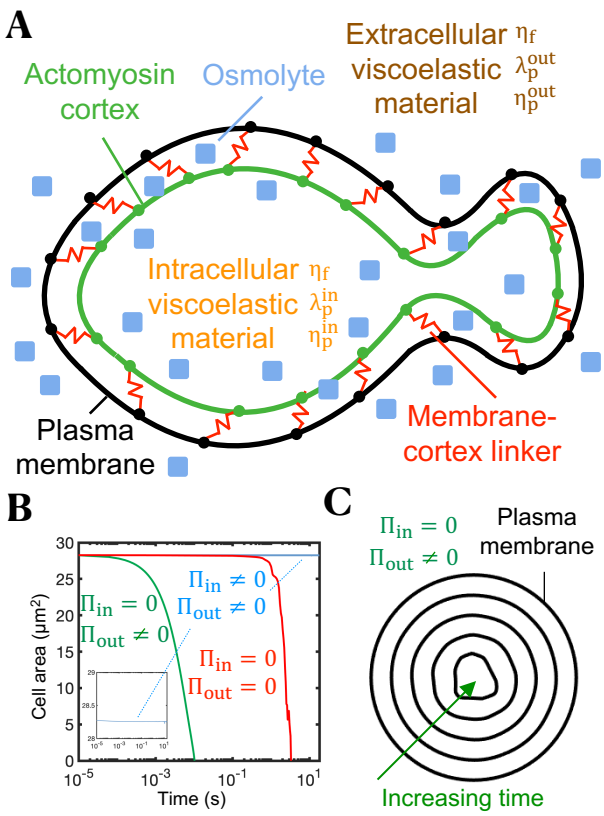

Figure 1. Intracellular osmotic pressure sets cell size and prevents cell shrinkage fostered by extracellular osmotic pressure and cortical tension. (A) Sketch of the bleb-based cell swimming model. Plasma membrane and actomyosin cortex are mechanically linked by reversible Hookean elastic linkers that stochastically associate and dissociate in a force-independent and -dependent manner, respectively. Intracellular and extracellular spaces are viscoelastic materials with associated fluid viscosity η_f, polymer viscosity η_p and polymer stress relaxation time λ_p. Osmotic effects are included. (B) Time-evolution of cell area for three different osmotic conditions. Intracellular osmotic pressure: Π_{in}, extracellular osmotic pressure: Π_{out}. (C) Cell shrinkage due to a reverse osmotic shock ($\Pi_{in} = 0$). Thus, inclusion of intracellular osmolytes is necessary to prevent cell collapse due to inward cortical tension and extracellular osmotic forces that tend to force water out of the cell.

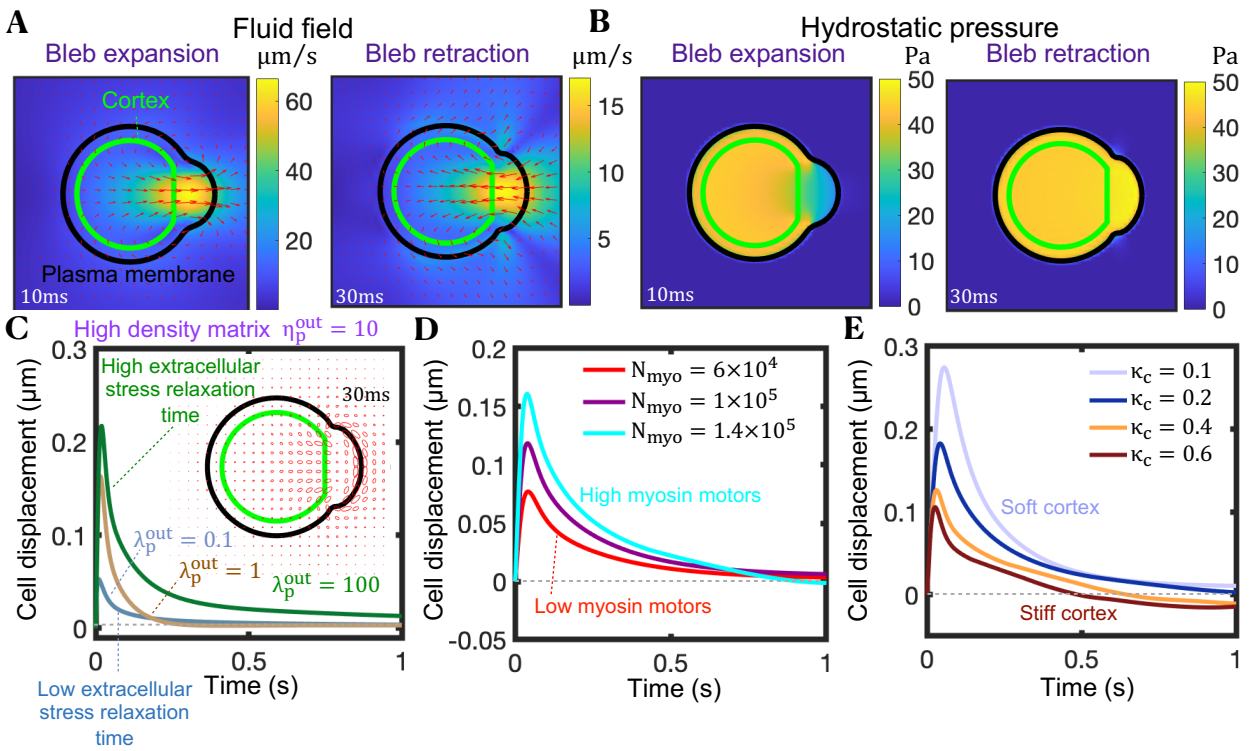

Figure 2. Net cell displacements during a single bleb cycle are insignificant. (A,B) Snapshots of the magnitude of the fluid velocity and velocity vectors (A), and hydrostatic pressure (B) acquired at two time-points during early bleb expansion and early retraction. (C) Time-evolution of the cell centroid for three different values of the extracellular stress relaxation time (in seconds). A short FENE-P stress relaxation time corresponds with a stiffer extracellular fluid. (C, inset) Ellipses represent the polymeric stress tensor $\boldsymbol{\sigma}_\mathbf{p}$ at a time-point during early bleb retraction. The major axis is aligned with the principal eigenvector of $\boldsymbol{\sigma}_\mathbf{p}$, with length scaled on the associated eigenvalue. The minor axis is associated with the second eigenvector of $\boldsymbol{\sigma}_\mathbf{p}$. The ellipses represent the directions and distension of the polymer field. Elastic stresses build up at the cell front and resist pressure-driven bleb expansion. (D,E) Time-evolution of the cell centroid for three different values of the number of myosin molecules inside the cell N_{myo} (D) and four different values of the cortical stiffness per unit of actin parameter κ_c (E). Greater cell displacements during bleb expansion are achieved for a softer and more contractile cortex. In all panels, membrane-

cortex linkers are broken by hand locally in a small region at time $t = 0$, mimicking a local downregulation of membrane-cortex linkers due to a chemical signal or force.

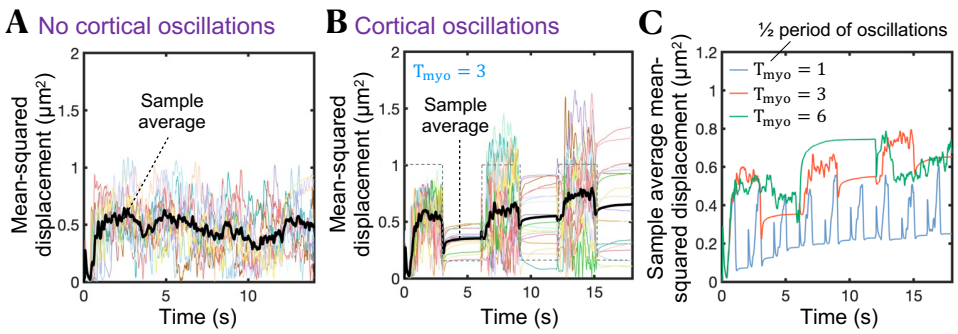

Figure 3. Cortical contractility oscillations are required for effective bleb-based cell swimming. (A,B) Time-evolution of mean squared displacement of 20 cells in the absence of cortical oscillations (A), and in the presence of cortical oscillations (B). The sample average over all cells (black line) increases over time for cells that produce cortical tension oscillations. Cells that do not produce cortical contractility oscillations are incapable of migrating effectively after the first bleb nucleation/expansion event. The gray dashed line in (B) indicates the waveform of the temporal oscillatory signal S_{osc}. (C) Sample average mean squared displacement over time for three different periods (in seconds) of the cortical contractility oscillation signal.

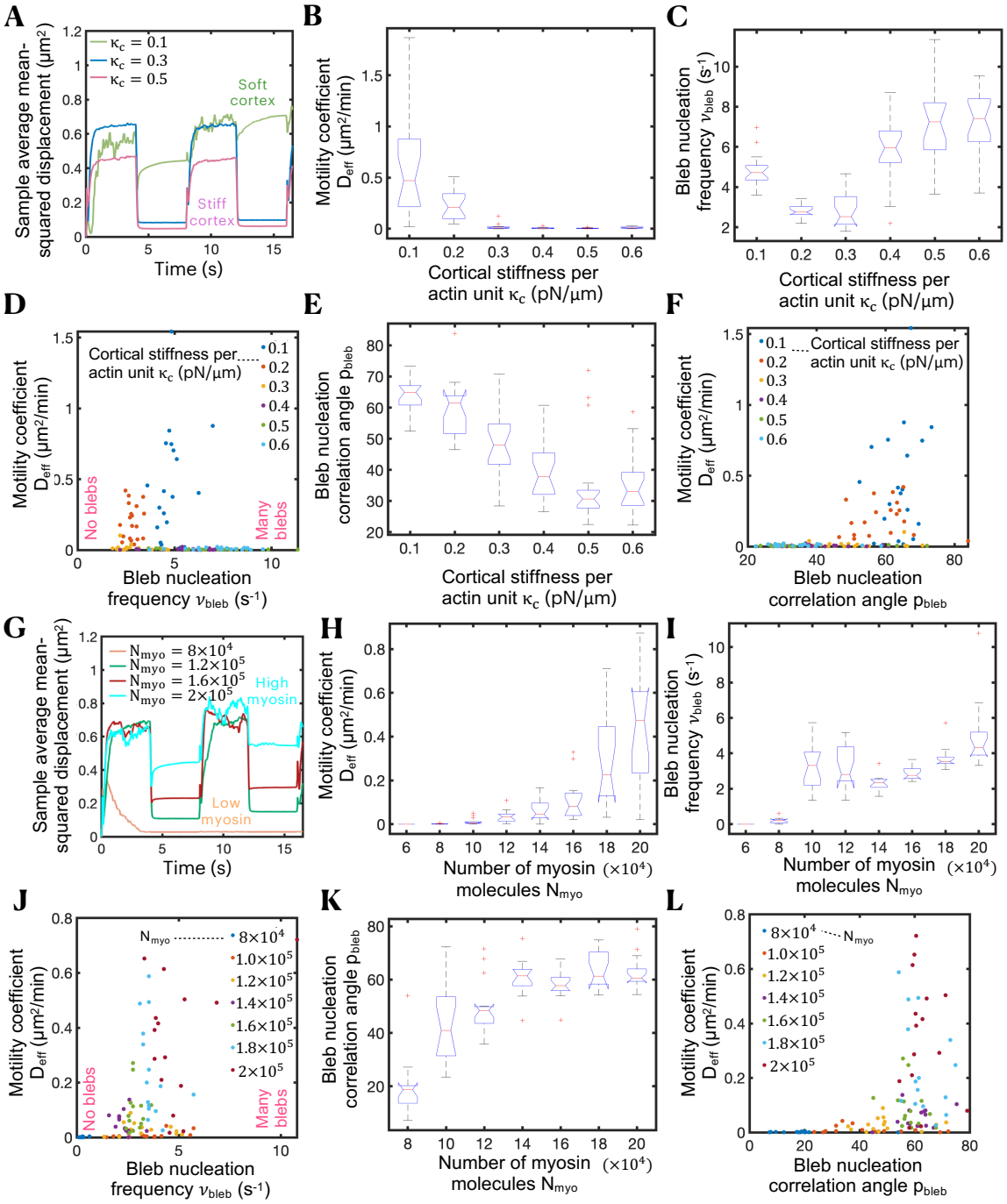

Figure 4. Swimming capabilities of bleb-producing cells can be modulated by cortical contractility and cortical stiffness. (A) Time-evolution of sample average mean squared displacement for four different values of the cortical stiffness per unit of actin parameter κ_c. (B,C) Effective random motility coefficient D_{eff} (B) and bleb nucleation frequency ν_{bleb} (C) as a function of κ_c. Cells swim more efficiently for lower cortex stiffnesses. D_{eff} is constrained to go through the origin in the

mean-squared-displacement-time plots. (D) Scatter plot showing the relationship between D_{eff} and ν_{bleb} for different values of κ_c. Intermediate bleb nucleation frequencies correlate with maximal random motility coefficients. (E) Polar angle between consecutive bleb nucleation events p_{bleb} as a function of κ_c. (F) Scatter plot showing the relationship between D_{eff} and p_{bleb} for different values of κ_c. Maximal random motility coefficients are observed for polar angles of ~60°-70°. (G) Time-evolution of sample average mean squared displacement for number of myosin motors N_{myo}. (H,I) Effective random motility coefficient D_{eff} (H) and bleb nucleation frequency ν_{bleb} (I) as a function of N_{myo}. Cells swim more efficiently for high number of motors. (J) Scatter plot showing the relationship between D_{eff} and ν_{bleb} for different values of N_{myo}. (K) Polar angle between consecutive bleb nucleation events p_{bleb} as a function of N_{myo}. (L) Scatter plot showing the relationship between D_{eff} and p_{bleb} for different values of N_{myo}. Maximal random motility coefficients are observed for polar angles of ~60°.

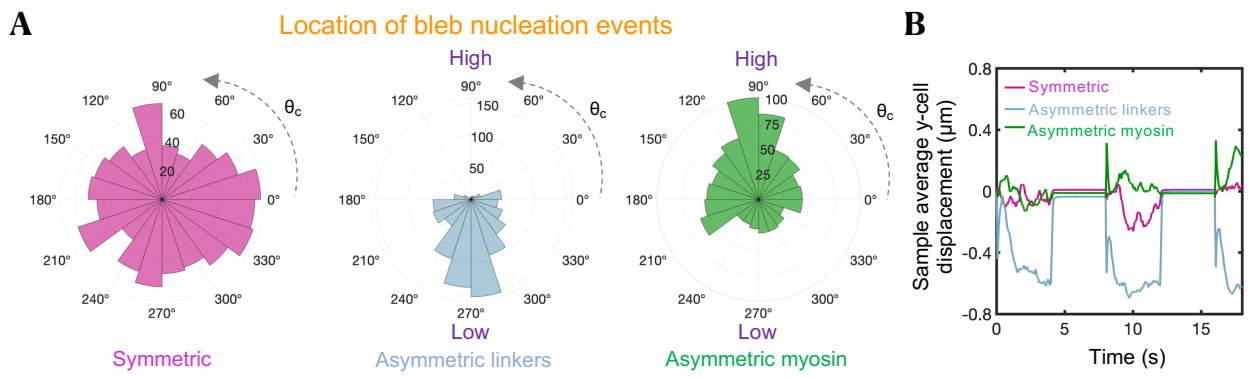

Figure 5. Blebs nucleate in regions of high myosin and low membrane-cortex linker levels. (A) Polar distribution of bleb nucleation events for three different conditions: uniform association of membrane-cortex linkers and myosin: $k^{on}_{adh_{eff}} = k^{on}_{adh}$, $k^{on}_{myo_{eff}} = k^{on}_{myo}$ (red violet), asymmetric kinetic association rate constant of membrane-cortex linkers: $k^{on}_{adh_{eff}} = k^{on}_{adh}(1 + 0.2 \sin \theta_c)$ (blue) and asymmetric kinetic association rate constant of myosin: $k^{on}_{myo_{eff}} = k^{on}_{myo}(1 + 0.2 \sin \theta_c)$ (green). Here, θ_c is the polar angle associated to each cortical node. (B) Time-evolution of sample average vertical cell displacements for the three different conditions.

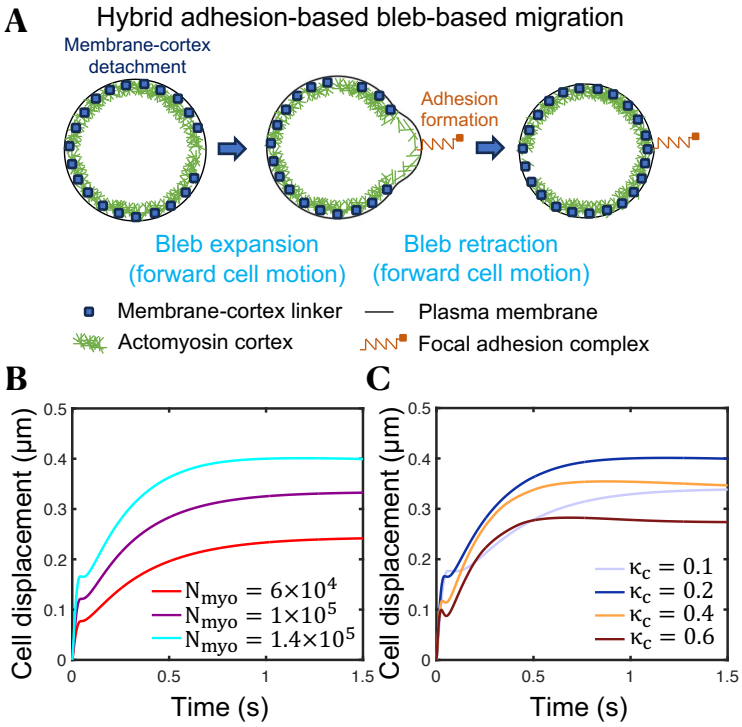

Figure 6. Cell-extracellular matrix adhesion is required for optimal bleb-based cell motility. (A) Visual representation of one complete cell migration cycle in the hybrid adhesion-based bleb-based mode of migration. (B, C) Time-evolution of the cell centroid for three different values of the number of myosin molecules inside the cell N_{myo} (B) and four different values of the cortical stiffness per unit of actin parameter κ_c (C). Larger cell displacements are achieved for elevated cortical tensions and intermediate cortical stiffnesses levels.

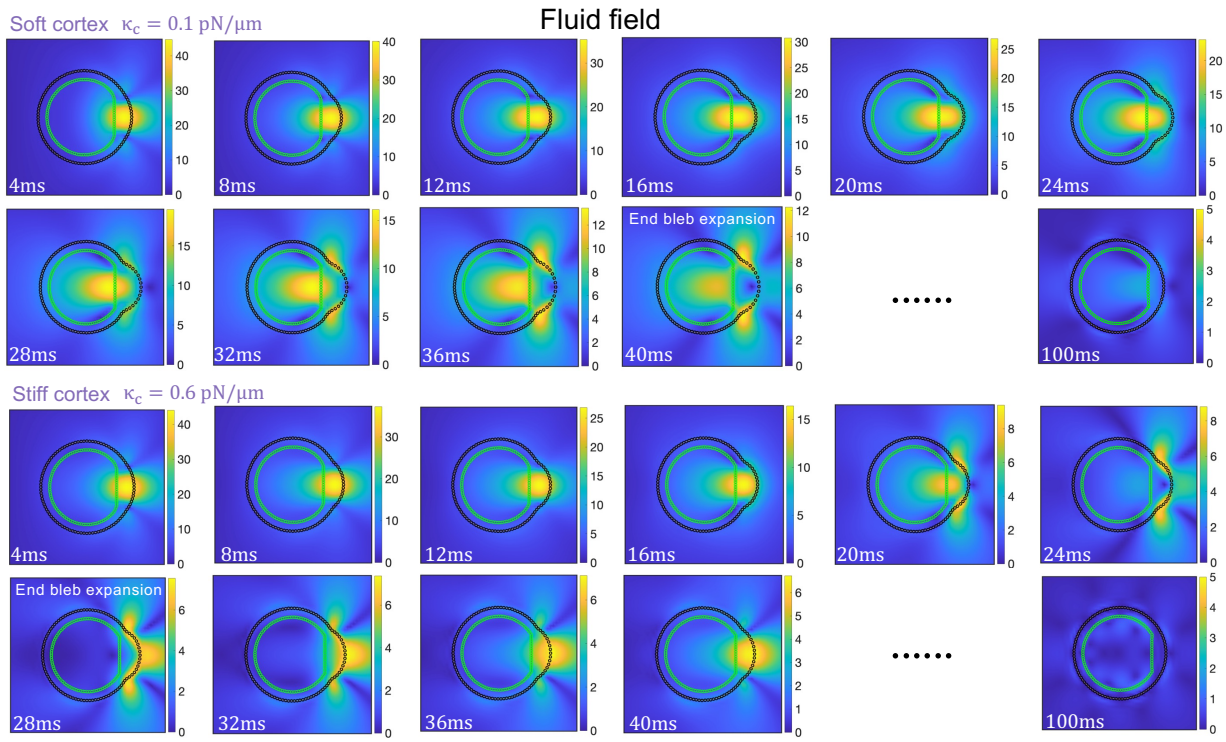

Figure S1A. Magnitude of the fluid field (□m/s) throughout a bleb cycle for two different values of the cortex stiffness per unit of actin parameter κ_c. Higher fluid velocities are observed for a softer cortex during both bleb expansion and bleb retraction. Membrane-cortex linkers are broken by hand locally in a small region at time $t = 0$, and are not allowed to break thereafter.

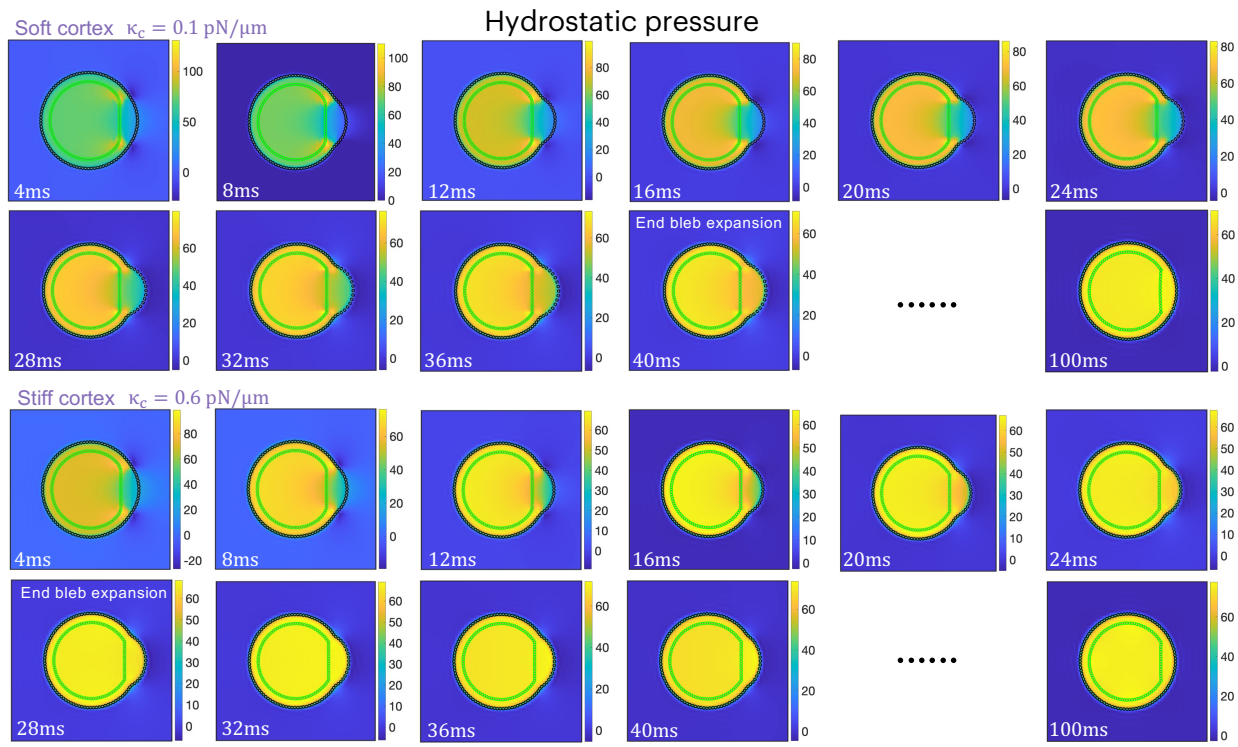

Figure S1B. Magnitude of the hydrostatic pressure (Pa) throughout a bleb cycle for two different values of the cortex stiffness per unit of actin parameter κ_c. Hydrostatic pressure equilibration and the end of bleb expansion occur at earlier times in the bleb cycle for a stiff cortex. Membrane-cortex linkers are broken by hand locally in a small region at time $t = 0$.

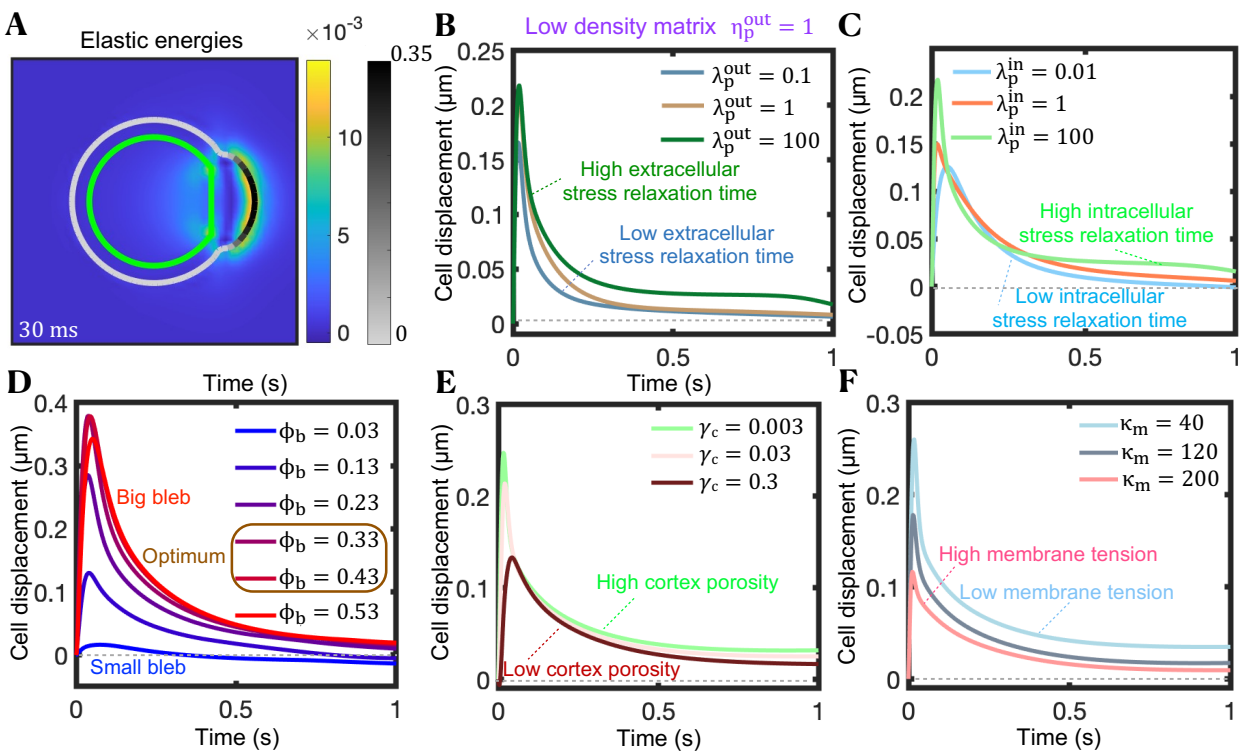

Figure S2. Elastic stresses and cortex-cytoplasm drag forces resist bleb expansion. (A) Mean-square distention of the immersed polymer material $\mathrm{tr}(\boldsymbol{\sigma}_\mathbf{p})$ and local membrane elastic energy at a time-point during bleb retraction. Regions of high polymer stress and membrane elastic tension buildup at the cell front. (B) Time-evolution of the cell centroid for three different values of the extracellular stress relaxation time (in seconds). Polymeric model parameter values: $\eta_p^{out} = 1\mathrm{pN} \cdot \mathrm{s} \cdot \square\mathrm{m}^{-1}$, $\eta_p^{in} = 1\mathrm{pN} \cdot \mathrm{s} \cdot \square\mathrm{m}^{-1}$, $\lambda_p^{in} = 100\mathrm{s}$. (C) Time-evolution of the cell centroid for three different values of the intracellular stress relaxation time. Polymeric model parameter values: $\eta_p^{out} = 0.1\mathrm{pN} \cdot \mathrm{s} \cdot \square\mathrm{m}^{-1}$, $\eta_p^{in} = 10\mathrm{pN} \cdot \mathrm{s} \cdot \square\mathrm{m}^{-1}$, $\lambda_p^{out} = 100\mathrm{s}$. (D–F) Time-evolution of the cell centroid for different values of the fraction of the cell membrane perimeter (bleb size) ϕ_b that loses mechanical connection with the underlying cortex (D), for different values of the cortex-cytoplasm viscous drag coefficient γ_c $(\mathrm{pN} \cdot \mathrm{s} \cdot \square\mathrm{m}^{-1})$ (E), and for different values of the plasma membrane spring stiffness κ_m $(\mathrm{pN} \cdot \square\mathrm{m}^{-1})$ (F). Intermediate bleb sizes, high cortex porosities and low plasma membrane stiffness maximize cell displacements during bleb expansion. In all panels, membrane-cortex linkers are broken by hand locally in a region set by ϕ_b at time $t = 0$.

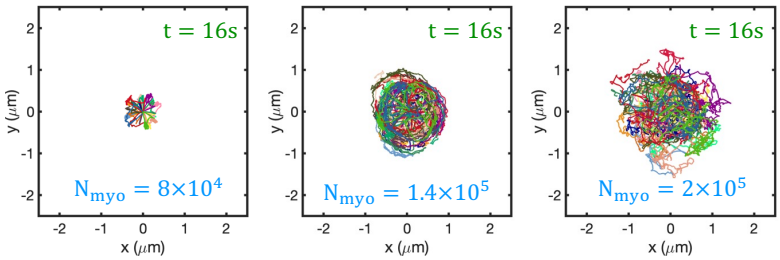

Figure S3. High contractile bleb-producing cells swim more efficiently. Wind rose plots depicting the migratory tracks of cells for three different myosin levels. Each color represents a single-cell trajectory.

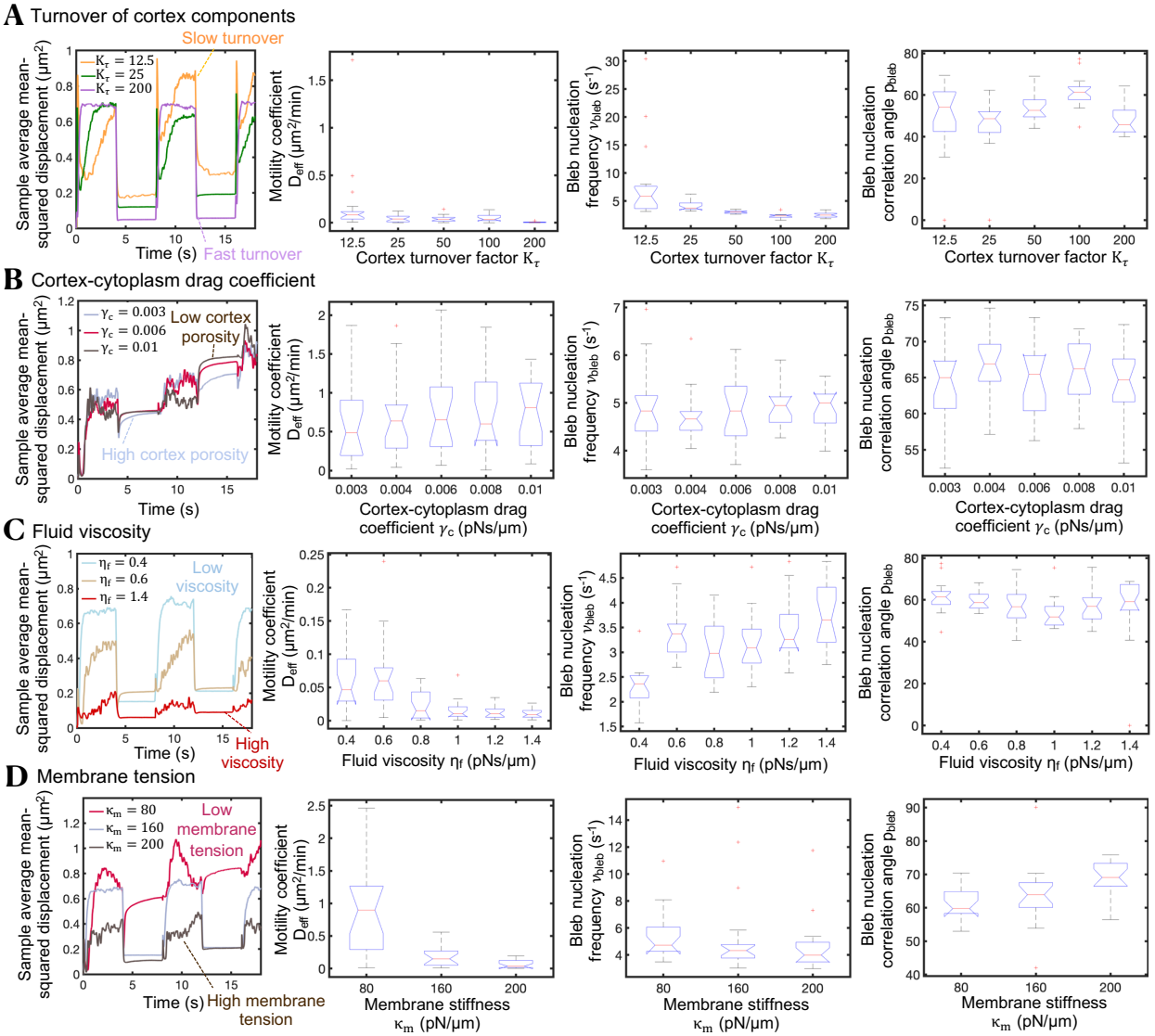

Figure S4. Cortex turnover, cortex porosity, fluid viscosity and membrane tension modulate bleb-based cell swimming capabilities. (A–D) Sample average mean-squared displacement, random motility coefficient D_{eff}, bleb nucleation frequency ν_{bleb}, and polar angle between consecutive bleb nucleation events p_{bleb} for different values of the (A) cortex turnover factor K_τ, (B) cortex-cytoplasm drag coefficient γ_c ($pN \cdot s \cdot \square m^{-1}$), (C) fluid viscosity η_f ($pN \cdot s \cdot \square m^{-1}$) and (D) membrane spring stiffness parameter κ_m ($pN \cdot \square m^{-1}$).

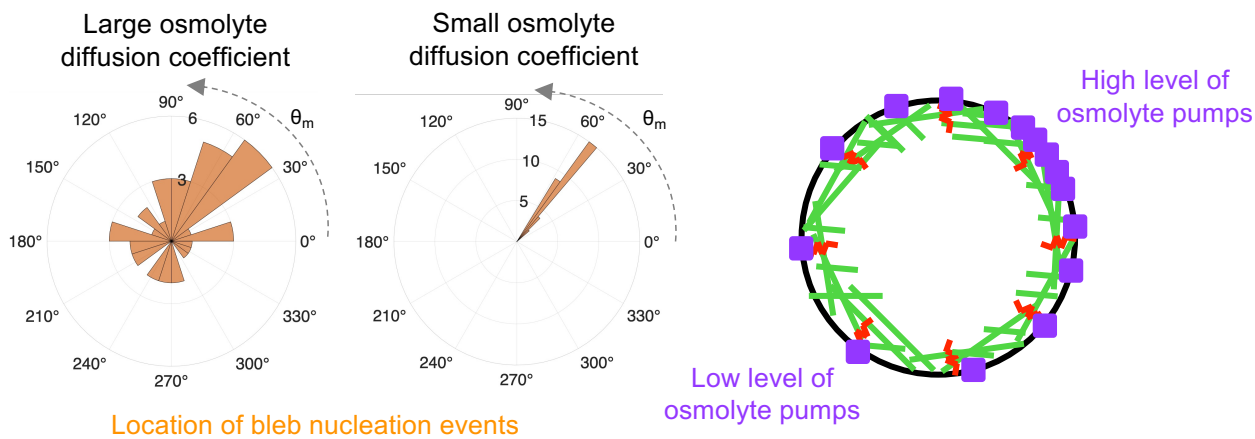

Figure S5. Blebs nucleate in high osmotic pressure regions. (A) Polar distribution of bleb nucleation events for fast osmolyte diffusion ($D_{in} = 500\mu m^2/s$) and slow intracellular osmolyte diffusion ($D_{in} = 5\mu m^2/s$), for an asymmetric osmolyte active pumping influx $\alpha_{pump}(s_j, t) = 10^7 \sin\theta_{m_j} \cos\theta_{m_j}$, where θ_{m_j} is the polar angle associated to the jth membrane node. Parameter values: $D_{out} = 2D_{in}$ and $\alpha_{passive} = 10^{-3}$.